Supplemental Material

Highly tunable multilevel resistive states in $VO_2/CuInP_2S_6$ heterojunction combining ionic migration and metal-insulator transition

Qiong Wu[a], Yanqing Zhang*[b], Kaihan Shan[a], Weiting Meng[a], Di Wang[a], Wenyu Jiang[a], Weiming Xiong*[a]

[a]Guangxi Key Laboratory for Relativity Astrophysics, School of Physical Science & Technology, Guangxi University, Nanning 530004, China

[b]Guangxi Key Laboratory of Information Functional Materials and Intelligent Information Processing, School of Physics & Electronics, Nanning Normal University, Nanning 530004, China

Corresponding authors.

Email: xiongwm3@gxu.edu.cn (W. Xiong)

Email: zhangyq66@nnnu.edu.cn (Y. Zhang)

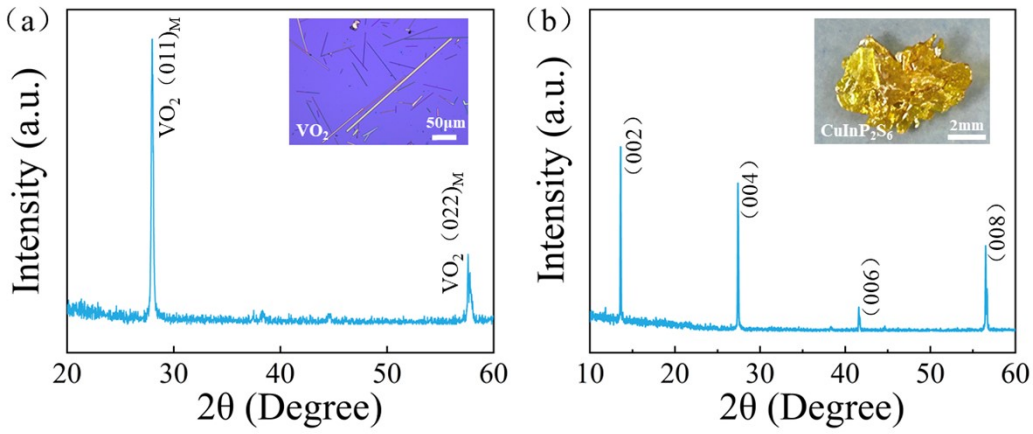

Fig. S1. (a) XRD diffractogram of the as-grown VO_2 microwires. The inset shows optical image of the as-grown VO_2 microwires. (b) XRD diffractogram of the as-grown bulk CIPS. The inset shows photograph of selected sample.

The XRD diffractogram (**Fig. S1**a) indicates that the high crystalline quality of the as-grown VO_2 microwires. Only (011) and (022) peaks of VO_2 monoclinic (M1) phase (JCPDS card 72-0514) are detected, revealing that the uniform growth orientation of VO_2 microwires. VO_2 microwires have smooth surfaces and lengths ranging from tens to hundreds of microns, as shown in the inset in **Fig. S1**a. Additionally, in **Fig. S1**b, the XRD diffractogram shows the the presence of (002), (004), (006) and (008) peaks of CIPS nanosheets, where the appearance of the (004) peak corresponds to CIPS ferroelectric phase. Therefore, it is evident that the synthesized bulk CIPS exhibits high crystallinity and purity. Also, the selected sample is displayed in the inset in **Fig. S1**b.

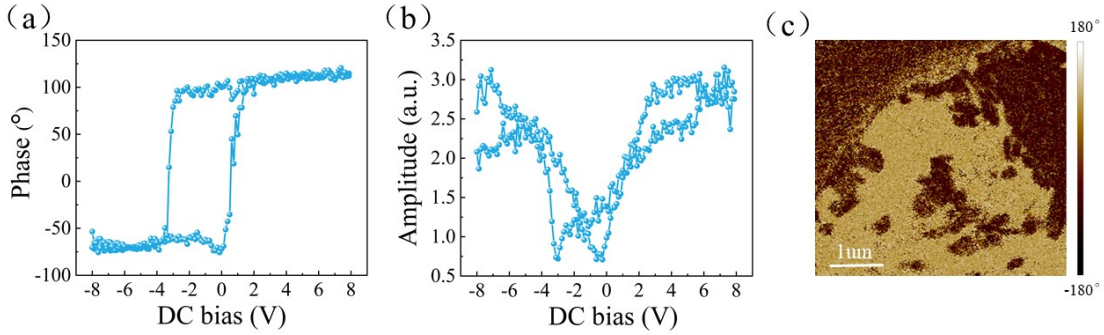

Fig. S2. Measured (a) phase hysteresis and (b) amplitude loops during an electric field sweeping loop by PFM. (c) Phase image of the ferroelectric domain of CIPS nanosheet.

Ferroelectric properties are characterized by piezoelectric force microscope (PFM). A standard phase hysteresis loop and piezoelectric amplitude "butterfly" curve are obtained (**Figs. S2**a and **S2**b), exhibiting significant out-of-plane ferroelectric polarization switching hysteresis. Besides, the phase image (**Fig. S2**c) of CIPS nanosheet shows clear ferroelectric domain patterns with two out-of-plane polarization states. These results demonstrate that the CIPS has an excellent ferroelectric property.

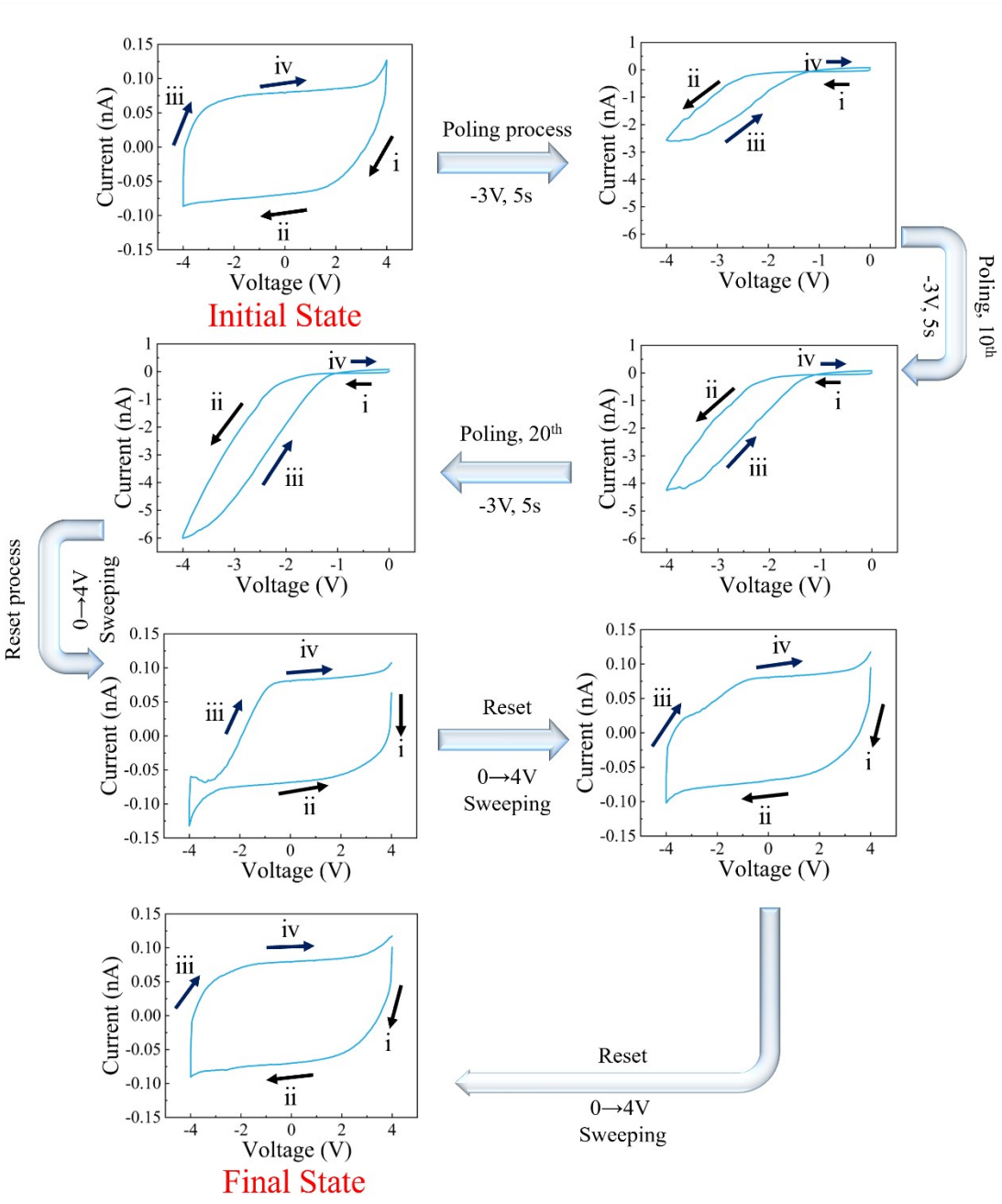

Fig. S3. The entire process of switching the device from the initial state (HRS) to the poling state (LRS), and then back to the initial state.

VO_2/CIPS heterojunction demonstrates tunable completing set and reset switching operations, achieving bidirectional threshold RS behavior. Initially, as the scanning voltage is swept from 4 V→0→-4 V, the as-fabricated VO_2/CIPS heterojunction exhibits a high resistance state (HRS) with a current value of about 0.1 nA. In this case, the distribution of Cu^+ in CIPS is randomly distributed uniformly, and the current curve is symmetrically distributed. Then, a negative bias with voltage of -3V and duration of

5 s is applied for poling, and within a scanning range (0→−4 V→0), the current value of the VO_2/CIPS heterojunction increases to 2.5 nA. At this situation, the VO_2/CIPS heterojunction switches to a low resistance state (LRS), which is attributed to the continuous directional migration of Cu^+ ions in CIPS under the electric field. With the increase of the poling cycle, more Cu^+ ions move in a directional direction and assemble near the cathode surface. When the number of poling cycles reaches 10^{th} and 20^{th} (5 s, -3 V), the current value of the device increase to 4 and 6 nA, respectively, which is more than 40 times higher than the initial state. While, when positive sweep voltages are applied, Cu^+ ions are driven back to their original uniform distribution, and the VO_2/CIPS heterojunction switches back to the HRS state. Consequently, the process of voltage scanning from 0→4 V is employed as a reset process. After multiple reset processes, the device eventually returned to a relatively stable state consistent with its initial state. The complete cycle process illustrates the reversible switching behavior between HRS and LRS in the device.

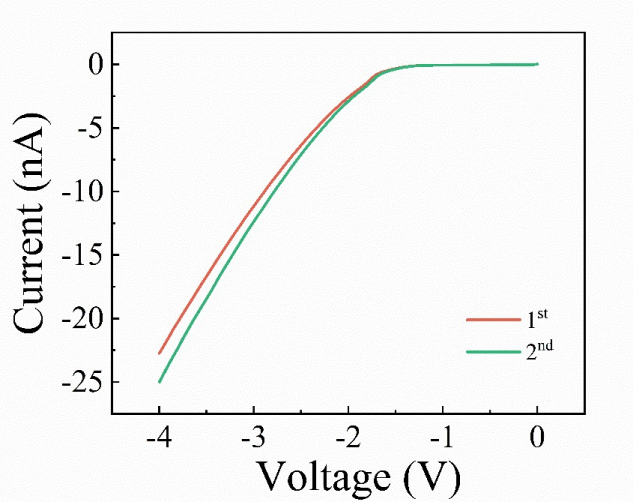

Fig. S4. I-V curves of device at voltage of -4 V for 15 s

Figure S4 shows the I-V curve of device at voltages of -4 V for 15 s. When the first sweep voltage is applied, the current value of VO_2/CIPS heterojunction is about 22 nA. As the scanning voltage is stimulated, the device current increases. The current value reach 25 nA after the 2^{nd} voltage scanning. Compared with the sweeping voltage of -4 V for 10 s (see **Fig. 3**e in the main text), the voltage duration of 15 s does not

cause a sharp change in current. This is because under the continuous stimulation of voltage above -4 V for 10 s, Cu^+ ion migration has basically stabilized, and no more Cu^+ ions move to the cathode.

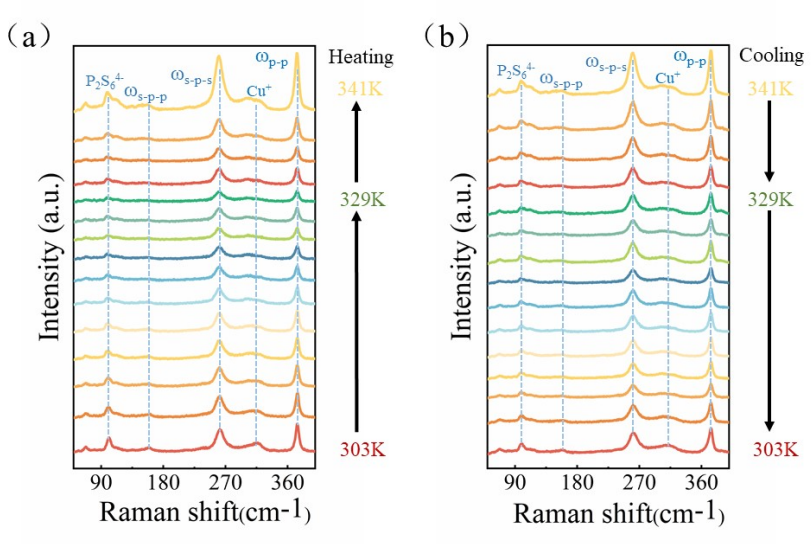

Fig. S5. Temperature-dependent Raman spectrums of CIPS. (a) Heating and (b) Cooling processes.

To investigate the effect of temperature on CIPS nanosheet, temperature-dependent Raman spectrums of CIPS during heaing and cooling process are shown in **Fig. S5.** Peaks at 266 and 376 cm^{-1} correspond to S-P-S and P-P phonon vibrations of CIPS. The Raman spectra demonstrate that temperature affects the intensity of diffraction peaks. During the heating process, the peak intensity of above two peaks decreased significantly around 329 K. This is attributed to the CIPS undergoes a transition from the ferroelectric phase to the paraelectric phase, with the peak intensity significantly inhibited near the transition temperature. While, with the increase of temperature, the peak intensity increase again. Similarly, during the cooling process, The peak intensity decreases near 329 K. A reversible transformation from paraelectric to ferroelectric phase can be achieved. The results indicate that CIPS exhibits a reversible ferroelectric-paraelectric phase transition.

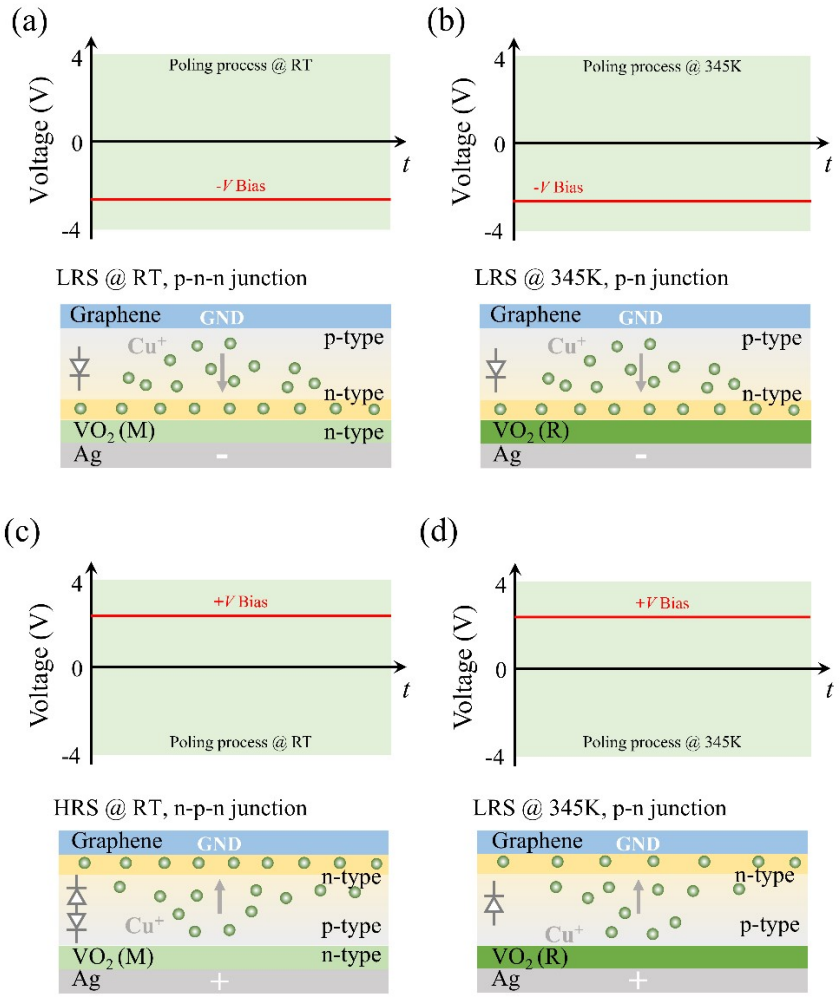

Fig. S6 The voltage application processes and the schematic diagrams of Cu^+ ions distributions under the (a) negative poling bias at RT, (b) negative poling bias at 345 K, (c) positive poling bias at RT and (d) positive poling bias at 345 K. The inhomogeneous distributions of Cu^+ ions driven by the negative poling bias result in the formation of n-p junction at RT and 345K. While, when under the positive poling bias, an n-p-n junction is formed at RT, and a p-n junction is formed at 345K, respectively.

When a poling process with a negative bias is continuously applied to the device at RT, the Cu^+ ion in CIPS should be redistributed to near VO_2 surface, resulting in the enrichment of Cu^+ ion near the cathode and the lack of Cu^+ ions near the graphene electrode terminal. Therefore, a p-n junction is formed in CIPS. On the other hand, VO_2 with insulating phase is a natural n-type materials, and the CIPS/VO_2 heterojunction still exhibits the a p-n junction structure (Fig. S6a). When the temperature exceeds 345K, VO_2 transforms from the insulating M phase to the metallic R phase, the migration behavior of Cu^+ ions under negative poling bias also leads to the formation

of p-n junctions in CIPS (Fig. S6b). However, when a poling process with a positive bias is continuously applied to the device, Cu^+ ions move toward the graphene electrode and accumulate at the cathode, forming a reverse p-n junction (i.e., n-p junction) in CIPS. At this situation, the n-p junction combines with insulating VO_2 to form an n-p-n structure at RT (Fig. S6c). When the temperature reaches 345 K, VO_2 changes from the insulating M phase to the metallic R phase, resulting in richer Cu^+ ion aggregation near graphene electrode, and CIPS still maintains the n-p junction (Fig. S6d). While, since the electrodes at both sides of CIPS are graphene and metal phase VO_2 respectively, and the different contact barrier between the CIPS and the electrodes at both ends leadthe Cu^+ ions in Fig. S6d and Fig. S6b showing different distribution.

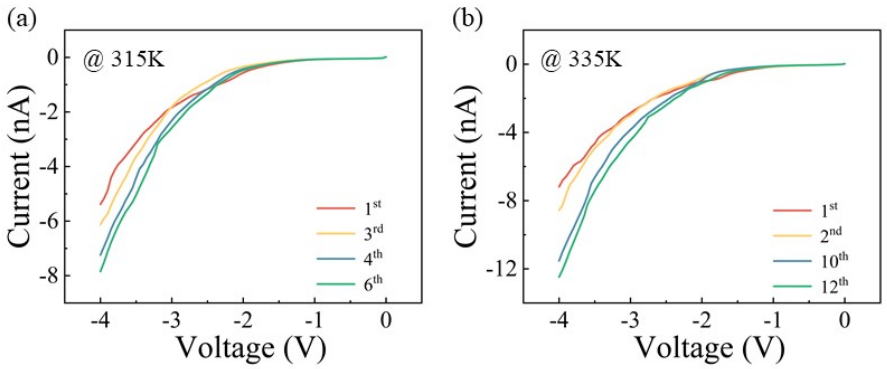

Fig. S7 Temperature-dependent I-V curves measured after the poling with bias of -3 V and duration of 5 s, (a) 315K, (b) 335 K.

The temperature-dependent I-V curves measured after the poling (-3 V, 5 s) are displayed in Fig. S7. When the temperature reaches 325 and 335K, the device current increases slightly compared with that at RT. And the device current increases with the poling cycles. It is worth noting that, regardless of how many cycles of poling processes are applied, the current still remains at the nA-level, which is also determined by the conductivity of the insulating M phase VO_2.

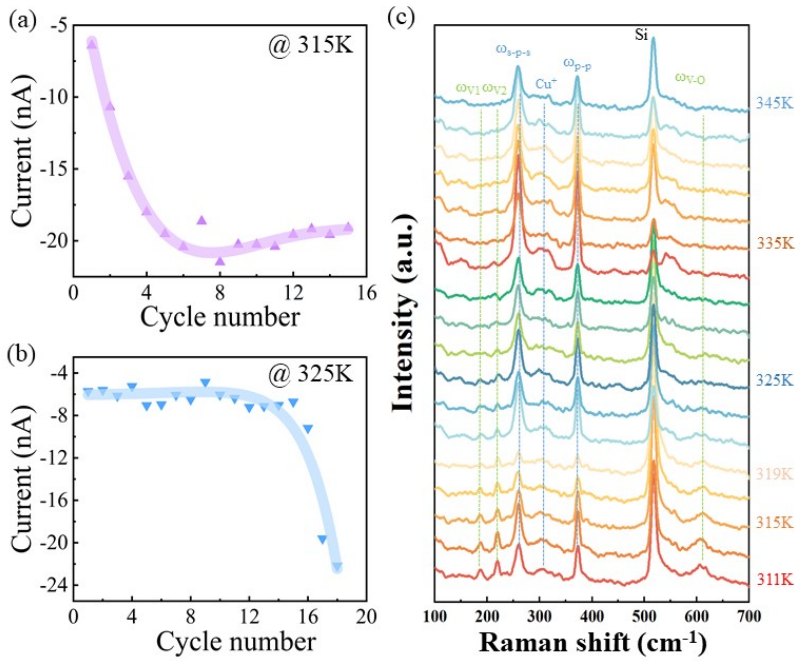

Fig. S8 Relationship between the measured current at -4 V and the poling cycle at (a) 315 K, (b) 325K, and (c) temperature-depending Raman spectra of CIPS sheet in the new sample of $VO_2/CuInP_2S_6$ heterojunction device.

Moreover, we have constructed another identical VO_2/CIPS heterojunction device, and perform the same temperature-dependent I-V characteristic measurements after the poling with bias of -3 V and duration of 5 s, as shown in Fig. S8a and Fig. S8b. The Curie temperature of the CIPS nanosheet in this VO_2/CIPS heterojunction device is between 315 and 325 K (Fig. S8c). When the temperature is lower than 315 K, the current rapidly increases at first several cycles and then tends to be saturated at a stable current. While, when temperature reaches 325K, the current remains stable at first several cycles and suddenly increases with the addition of the poling cycle. These results indicate that the ferroelectricity of CIPS plays an important role in measuring the curve of the relationship between the measured current and poling cycles. As we know, when the temperature is below Curie temperature, CIPS nanosheet exhibits a good ferroelectricity, the ferroelectric-polarization-induced built-in electric field promote the accumulation of Cu^+ ion. Through the synergetic contribution of ferroelectric polarization and applied bias poling cycles, only a few poling cycles are needed to drive the current to rapidly increase and reach saturation. While, when the temperature is above Curie temperature, CIPS transforms into the paraelectric phase

and will not exhibit the built-in electric field caused by ferroelectric polarization. In this situation, only the poling bias drives the migration of Cu^+ ions, so more poling cycles are required to achieve a larger current state.

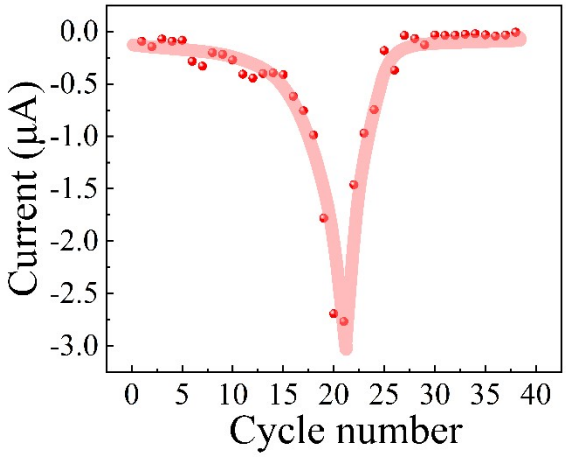

Fig. S9 Relationship between the measured current at -4 V and the overload poling cycle (-3V, 5s) at 345 K.

The relationship between the measured current at -4 V and the overload poling cycle (-3V, 5s) at 345 K is studied in this work. According to the above analysis, voltage cycle stimulation can effectively modulate Cu^+ ions migration to achieve a tunable device conductance response. As the poling cycle increases, the current of VO_2/CIPS heterojunction device increases gradually. It should be emphasized that, when the current reaches maximum value after several poling processes (i.e., 21 poling cycles), a reduced current is observed with the continuesly increase of poling cycles (Fig. S9), which is caused by an irreversible Cu^+ loss occurring in CIPS[S1]. Therefore, to avoid this harmful reaction, the bias poling cycles should be well considered.

Reference

S1 Y. Huang, S. Yao, F. Sun, X. Zhang, W. Chen, X. Liu and Y. Zheng, Cu^+ migration and resultant tunable rectification in $CuInP_2S_6$, *ACS Appl. Electron. Mater.*, 2023, **5**(10), 5625-5632, DOI: 10.1021/acsaelm.3c00973.